

Applications of Mathematics

Ivan Saxl; Petr Ponižil

Bernoulli cluster field: Voronoi tessellations

Applications of Mathematics, Vol. 47 (2002), No. 2, 157–167

Persistent URL: <http://dml.cz/dmlcz/134492>

Terms of use:

© Institute of Mathematics AS CR, 2002

Institute of Mathematics of the Czech Academy of Sciences provides access to digitized documents strictly for personal use. Each copy of any part of this document must contain these *Terms of use*.



This document has been digitized, optimized for electronic delivery and stamped with digital signature within the project *DML-CZ: The Czech Digital Mathematics Library* <http://dml.cz>

BERNOULLI CLUSTER FIELD: VORONOI TESSELLATIONS*

IVAN SAXL, Praha, PETR PONÍŽIL, Zlín

Abstract. A new point process is proposed which can be viewed either as a Boolean cluster model with two cluster modes or as a p -thinned Neyman-Scott cluster process with the retention of the original parent point. Voronoi tessellation generated by such a point process has extremely high coefficients of variation of cell volumes as well as of profile areas and lengths in the planar and line induced tessellations. An approximate numerical model of tessellation characteristics is developed for the case of small cluster size; its predictions are compared with the results of computer simulations. Tessellations of this type can be used as models of grain structures in steels.

Keywords: cluster point process, Voronoi tessellation, induced tessellation, coefficients of variation of cell size characteristics

MSC 2000: 60–04, 60D05, 60G55

1. INTRODUCTION

The tessellation (or tiling) T^d is a covering of \mathbb{R}^d by a countable family of closed subsets (cells, tiles) $C_i \in \mathbb{R}^d$, $i = 1, 2, \dots$, which is a packing at the same time. Consequently, the cells have disjoint interiors and their union is \mathbb{R}^d . A closely related but much more complicated problem are finite coverings and packings where the packed and covered ground set A is a bounded subset of \mathbb{R}^d only. The latter problem is much closer to practical tasks but the effects occurring near the boundary of A are formidable. Hence a great advantage is gained if the covering and packing of a bounded set A can be regarded as an intersection $A \cap T^d$.

There is a good reason to study tessellations because there are many natural divisions of the space (crystalline solids, cellular tissues) as well as artificial ones created

* This work was supported by the Grant No. 201/99/0269 of the Grant Agency of the Czech Republic (the first author) and by the Grant No. 96108 of the Ministry of Education of the Czech Republic (the second author).

by human activities (countries, jurisdictions, districts of administration, allotments). As general references for random tessellations see Okabe et al. [4], Stoyan et al. [11], Møller [2], [3].

In the present paper, convex random Voronoi tessellations are considered as a model of the natural space-filling structure formed by grains of polycrystalline metals. In particular, the main topic of interest are tessellations with a great nonuniformity of the cell size. As the metals are opaque and the grain separation nearly impossible, only a partial information on T^3 is accessible, namely the induced tessellations $T^k = T^d \cap F_k^d$, $k < d$, where F_k^d is the k -flat in \mathbb{R}^d . The notation T' , T'' for $k = 2, 1$ will be used in what follows for tessellations induced by T^3 in section planes and lines, respectively.

The main size or scale characteristic of a tessellation is its *intensity* λ —the mean number of cells (equivalently, of their generators) per unit volume of the embedding space; λ' , λ'' are then the intensities of induced tessellations T' , T'' , respectively.

A detailed description of a tessellation is given by the distributions of its cell characteristics. The size dependent characteristics are homogeneous functions of the degree $-k/d$ of the intensity $\lambda = 1/\mathbf{E}v$, where $k = d$ for the cell content v , $k = d - 1$ for the cell surface content s , and $k = 1$ for the mean cell breadth w (the mean length of cell projections into an isotropic bundle of 1D linear subspaces of the embedding space). The shape characteristics like the number of cell faces n_f are independent of λ ; $k = 0$. Similarly for the T' induced tessellation $\lambda' = 1/\mathbf{E}v'$, where v' is the area of the induced cell (called the profile), the other size characteristics are the perimeter s' and the mean breadth w' mutually related by the Cauchy relation $s' = \pi w'$. Finally, $\lambda'' = 1/\mathbf{E}v''$ in T'' , where v'' is the section (chord) length. Because of the homogeneity property of the size characteristics with respect to the intensity λ , it is sufficient to consider only the unit tessellations ($\lambda = 1$).

The scale of grain size and arrangement of technical materials is extremely wide. Whereas grains are usually rather uniform equiaxial in pure metals and alloys with close packed face-centred cubic and hexagonal lattices, like copper, aluminium, zinc etc., grain structures of steels after various thermal treatments are extremely variable with two or even more components of widely different sizes and arrangements. Consequently, a sufficiently wide class of model tessellations must be developed in order to cover a representative sample of natural tessellations occurring in practice. The simplest possible common parameters serving as a basis of comparison between model and real tessellations are the coefficients of variation $\text{CV } v$, $\text{CV } v'$ and $\text{CV } v''$. A study of rather common steels after various thermal treatments revealed that $\text{CV } v'$ can be as high as 3 and also $\text{CV } v'' > 1.1$ must be expected [13]. The lower bounds on these coefficients of variations are their values corresponding to monohedral tessellations of cells (grains) the shape of which approaches a ball (tetrakaidecahedron,

rhombic dodecahedron). On the opposite side there are multimodal grain structures with regions of small grains separated by overgrown grains of size greater by several orders of magnitude. The present model has been developed just in order to hit off the latter situation.

2. VORONOI TESSELLATIONS GENERATED BY BERNOULLI POINT CLUSTER FIELDS

A random Voronoi tessellation is constructed from a given random point process Φ by adjoining to every point $x_i \in \Phi$ the cell formed by all points y of the embedding space \mathbb{R}^d such that $\|x_i - y\| \leq \|x_j - y\|$ for all $x_j \in \Phi$, $x_j \neq x_i$. The point cluster field Ψ is created by applying the operation of clustering to a given parent point process Φ_p , namely by replacing every point $x_i \in \Phi_p$ by a point cluster $Z \oplus x_i$ [11], [12]. Φ_p is usually a stationary Poisson point process (PPP) of intensity λ_p . First, the definition is necessary of point clusters used in what follows.

Let \mathcal{Z} be the class of all finite point sequences $Z \in \mathbb{R}^d$. A random element $Z \in \mathcal{Z}$ with a distribution $P(Z)$ is a random cluster. A Poisson cluster is the support set of a (non-stationary) Poisson point process in \mathbb{R}^d with finite intensity measure Λ of expectation $N = \Lambda(\mathbb{R}^d)$ called the mean cluster cardinality. For any Borel set A , $\text{card}(A \cap Z)$ is a Poissonian random variable of mean $\Lambda(A)$. A cluster is called (Poisson) globular (PG) or spherical (PS), if

$$\Lambda(A) = \frac{N}{\nu_d(B_D)} \nu_d(B_D \cap A) \text{ or } \Lambda(A) = \frac{N}{\nu_{d-1}(\partial B_D)} \nu_{d-1}(\partial B_D \cap A),$$

respectively. Here $\nu_k(\bullet)$ is the k -dimensional Hausdorff measure and B_D is the ball of diameter D (centred at the origin \mathcal{O}). The points forming a cluster (called the daughters) are then dispersed either within B_D or on its boundary ∂B_D . Poisson globular and spherical clusters form a subclass \mathcal{Z}_{PGS} of \mathcal{Z} .

In the proposed model called the *Bernoulli cluster field* Φ (in analogy to the Bernoulli lattice process), the implantation of a point cluster $x_i \oplus Z$ is carried out with a fixed cluster probability $0 \leq p \leq 1$ (the point x_i is then removed) whereas only the point x_i is retained with the probability $1 - p$. Equivalently, the cluster Z has two modes: it is the above defined point cluster of PG or PS type—with the probability p —or the origin \mathcal{O} —with the probability $1 - p$. The process can also be looked upon as an independent p -thinning (with the retention of the original parent point x_i) of the ordinary cluster field Ψ . The intensity of the resulting point process Φ is $\lambda = (pN + 1 - p)\lambda_p$; if $p = 1$ then Φ is the Neyman-Scott cluster field with PG or PS clusters, if $p = 0$ then $\Phi = \Phi_p$ is the underlying point process (i.e. PPP). The

ball size D is expressed by the dimensionless parameter $\delta = D/\varrho_p$, where ϱ_p is the mean nearest neighbour distance of the parents ($\varrho_p = 0.554 \lambda_p^{-1/3}$ for PPP in \mathbb{R}^3).

Properties of tessellations generated by Neyman-Scott fields of PG or PS clusters have been examined in detail by Saxl and Ponížil [6], [7]. T^3 tessellations generated by PS fields have unimodal distributions of cell size characteristics and the cells are plate-like, rod-like and wedge-like. On the contrary, characteristics of tessellations generated by PG fields have strictly bimodal distributions whenever δ is small and $N > 5$. Besides outer cells with a volume v not much different from 1, also very small inner cells of a volume of $0.09 \delta^3$ are formed (Saxl and Ponížil [6], [7]). These inner cells are completely encircled by cells generated by points of the same cluster and their proportion α increases with growing N ; at $N = 99$ it is $\alpha \approx 0.6$.

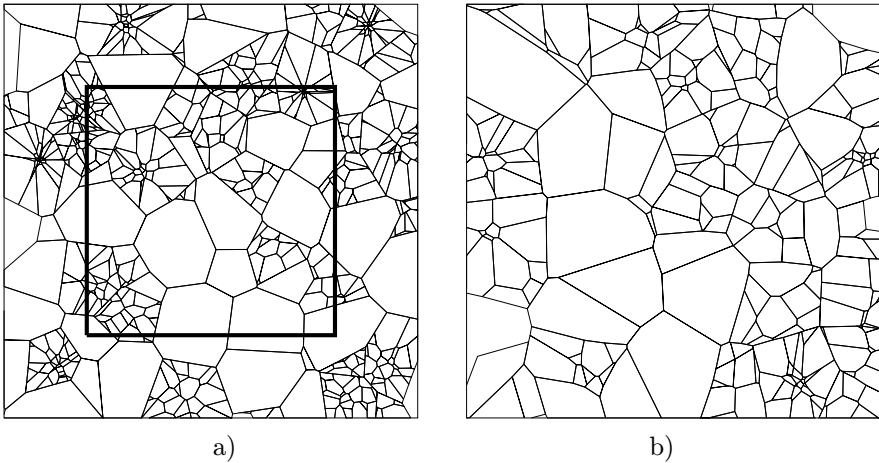


Figure 1. Planar sections (induced tessellations T') of T^3 tessellations generated by Bernoulli cluster fields with $p = 0.5$ and $\delta = 0.05$. a) T^3 generated by a BePS cluster field, $N = 70$ (a section of the cube in which the simulation was carried out; only the cells lying in the central part of the cube are considered in order to suppress the edge effects). b) T^3 generated by a BePG cluster field, $N = 50$ (only the cells hitting the measuring square window are shown).

These properties are naturally transposed also to tessellations generated by Bernoulli cluster fields. The choice $\delta \leq 0.1$ and high N produces a tessellation consisting of a $(1 - p) : p$ mixture of large and only slightly corrugated parent cells and of such cells fragmented into N small elongated cells. The 3D cell arrangement is clearly observable also from 2D planar sections—Fig. 1. The distribution of the cell volume is roughly bimodal with the mode ratio approximately $1 : N$ in the case of spherical clusters and trimodal in the case of globular clusters (with inner cells lying completely within the fragmented parent cell in a close neighbourhood of the parent point)—Fig. 2. Even when the spherical and globular cases have considerably

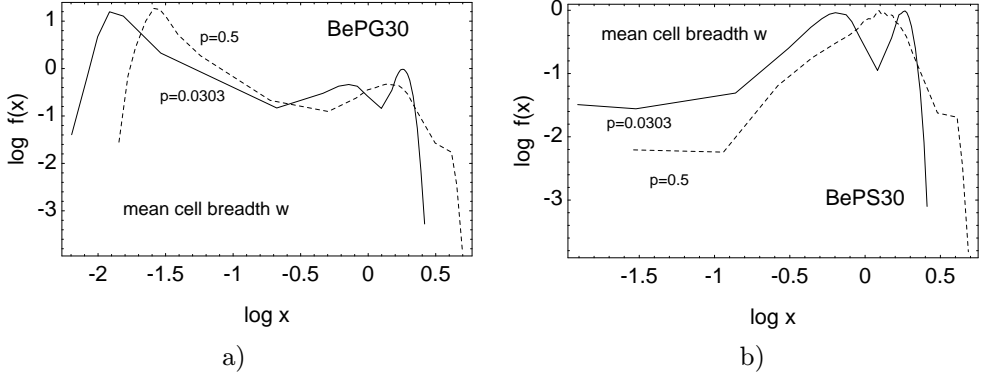


Figure 2. Trimodal tessellations generated by BePG cluster fields and bimodal tessellations generated by BePS cluster fields at two different values of the probability p .

different size properties (see below) they both give rather high values of the CV v and of other coefficients of variation.

The exact properties of tessellations must be found by computer simulation. However, a rough model can be proposed of the tessellation characteristic behaviour based on the known characteristics of the limit cases $p = 0$ —a Poisson-Voronoi tessellation (PVT) of intensity λ_p —and $p = 1$ —a tessellation generated by a Neyman-Scott cluster field of intensity $\lambda = N\lambda_p$. The model is suitable for sufficiently small values of δ ensuring only a negligible influence of partitioned cells on their non-partitioned neighbours.

Let us consider a tessellation characteristic, which is a homogeneous function of the degree $-k/d$ of the intensity λ . Let $\lambda_p = 1$, i.e. $\lambda = 1 + p(N - 1)$; neglecting the interaction of neighbouring parent cells, we may consider the resulting tessellation as a mixture of p cells containing a cluster of the mean cardinality N and $(1 - p)$ cells of the original parent process. Let q_k be the value of the considered characteristic in a unit cluster tessellation and Q_k its value in the unit PVT. Denoting by \tilde{q}_k the corresponding characteristic of the mixture, its j -th moment about origin can be written as (in the units of $\mathbf{E}\tilde{v} = 1$)

$$\begin{aligned}
 (1) \quad \mu'_j(\tilde{q}_k) &= \frac{Np \frac{\mu'_j(q_k)}{N^{jk/d}} + (1-p)\mu'_j(Q_k)}{\lambda} \lambda^{jk/d} \\
 &= \frac{N^{(d-jk)/d} p \mu'_j(q_k) + (1-p)\mu'_j(Q_k)}{\lambda^{(d-jk)/d}}.
 \end{aligned}$$

In order to simplify the formula, $m(q)$ will be introduced for $\mu'_j(q_k)/\mu'_j(Q_k)$ and c for $d - jk/d$. Then e.g.

$$(2) \quad \mu'_1(\tilde{w}) = \mathbf{E}\tilde{w} = \mathbf{E}W \frac{1 + p(N^c m(w) - 1)}{\lambda^c}, \quad c = 2/3,$$

and similarly for $\mathbf{E}\tilde{n}_f$, $\mathbf{E}\tilde{s}$, $\mathbf{E}\tilde{v}^2$ with $c = 1, 1/3$ and -1 , respectively. For $jk \neq 0$, i.e. $c \neq 1$, $\mu'_j(q_k)$ has an extreme at

$$(3) \quad p_e = \frac{1}{1-c} \left[\frac{c}{N^c m(q) - 1} - \frac{1}{N-1} \right].$$

$\mathbf{E}\tilde{v}^2$ has a maximum at

$$p_{\max} = \frac{1}{2} \left[1 + \frac{m(v^2)(N-1) - 2N}{(N - m(v^2))(N-1)} \right] \approx \frac{1}{2} \left[1 + \frac{m(v^2) - 2}{N - m(v^2)} \right] \text{ for high } N.$$

The second term in the brackets is of the order of 0.01, hence $p_{\max} \approx \frac{1}{2}$. Consequently, an approximate formula for $(CV v)_{\max} \approx \sqrt{0.3N - 1}$ (independently of $m(v^2)$) holds in a reasonable agreement with the accurate calculation—see Fig. 3. The corresponding values of $\{\mathbf{E}w, \mathbf{E}s\}$ at p_{\max} are shown in Fig. 4.

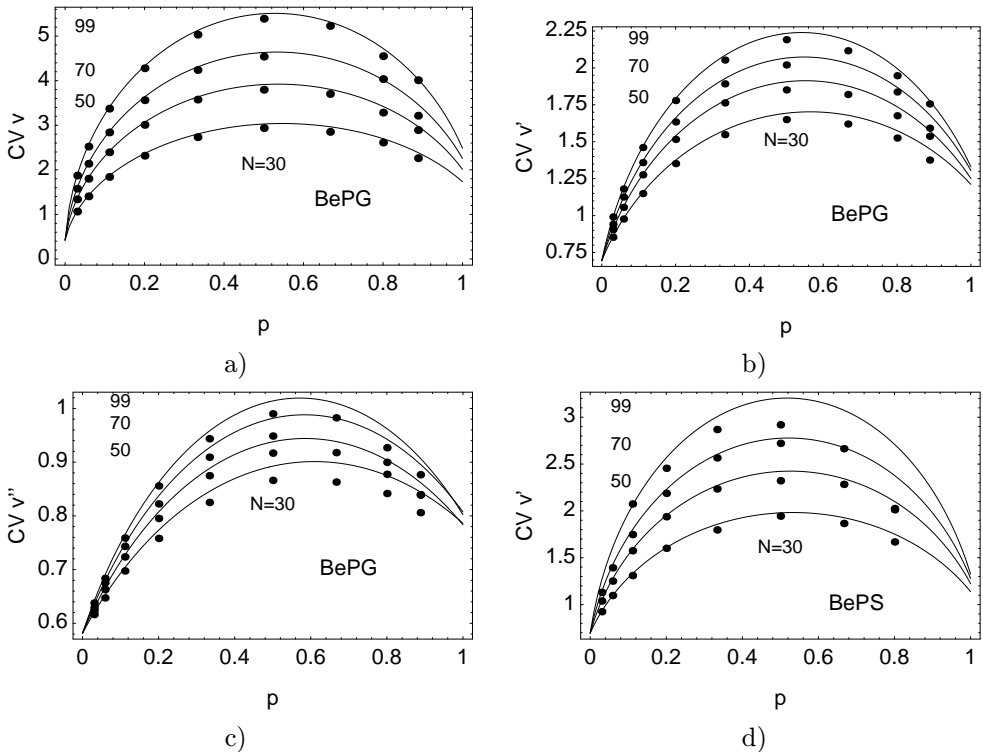


Figure 3. Coefficients of variation of tessellations generated by BePG and BePS cluster fields: the curves result from the approximate theory (Eq. (1)), the points show the estimates obtained by computer simulations.

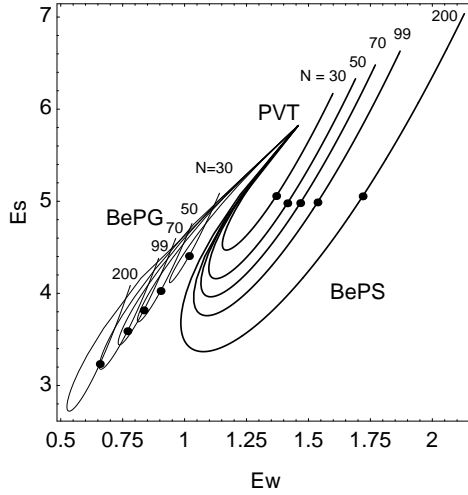


Figure 4. Bernoulli cluster field tessellations in the $w - s$ plane. The curves are parametrized by the probability $0 \leq p \leq 1$. The common end-point (PVT) corresponds to $p = 0$, whereas the loose $p = 1$ end-points delineate the curve $\{\mathbf{E}w, \mathbf{E}s\}_N$ characterizing the effect of the mean cardinality N on the position in the $w-s$ diagram for tessellations generated by Neyman-Scott cluster fields with spherical (right upper corner) and globular (medium quasi-diagonal part) clusters. The black points show the positions of maxima of CV v (the values ≈ 3.0 , ≈ 7.8 correspond to $N = 30$, 200 , resp., in both the BePG and BePS cases).

It follows from the above formulas that arbitrarily small values of $\mathbf{E}\tilde{w}$, $\mathbf{E}\tilde{s}$ and arbitrarily high values of $\mathbf{E}\tilde{v}^2$ can be achieved by choosing suitable values of parameters p and N (the tip of the BePG curve for $N = 999$ has coordinates $[\approx 0.3, \approx 1.8]$ and $CVv \approx 17$).

The present model obviously holds only if the changes in the original parent cells due to cluster implantation can be neglected, i.e. when the cluster size δ is small, very roughly if $\delta \leq 0.1$. The partial breakdown of the model at $\delta = 0.5$ and complete breakdown at $\delta = 2$ will be demonstrated below.

Also the mean values of induced tessellation size characteristics can be easily calculated. By the well known relations between the characteristics of a unit T^3 and T' , T'' (e.g. [10])

$$(4a) \quad \frac{1}{\lambda'} = \mathbf{E}\tilde{v}' = \frac{1}{\mathbf{E}\tilde{w}}, \quad \mathbf{E}\tilde{s}' = \frac{\pi}{4} \frac{\mathbf{E}\tilde{s}}{\mathbf{E}\tilde{w}},$$

$$(4b) \quad \frac{1}{\lambda''} = \mathbf{E}\tilde{v}'' = \frac{4}{\mathbf{E}\tilde{s}} = \pi \frac{\mathbf{E}\tilde{v}'}{\mathbf{E}\tilde{s}'}$$

An illustrative tool can be then introduced, namely the $w-s$ diagram in which any unit tessellation T^3 is described by a point $\{\mathbf{E}w, \mathbf{E}s\}$. The $w-s$ diagram can also be understood as a $\lambda'-4\lambda''$ diagram, or, equivalently, as an $(\mathbf{E}\tilde{v}')^{-1}-4(\mathbf{E}\tilde{v}'')^{-1}$ diagram;

this is a direct consequence of Eqs. (3). The w - s diagram of the Bernoulli cluster tessellations constructed by using the above given formulas is shown in Fig. 4. The different shapes of BePG and BePS curves follow from dissimilar values of $m(q)$, $q = w, s$. Namely, $m(q) \leq 1$ in the former case and $m(q) \geq 1$ in the latter one. The minimum values of $\mathbf{E}s$ (tips of the curves in Fig. 4) are attained at the values $p_{\min}(s)$ given by Eq. 3; they decrease with growing $30 \leq N \leq 200$ within the ranges $\{0.17, 0.07\}$ and $\{0.24, 0.15\}$ for BePS and BePG, respectively.

In order to calculate the coefficients of variation of 2D profile areas and 1D profile lengths, the individual contributions of small and large fraction profiles must be separated. Sampling of cells by sectioning flats is not uniform but weighted by the cell properties, namely by w and $s/4$ in the planar and line sections, respectively. Consequently, the number ratio of small and large cells in the original 3D tessellation is $r = pN/(1-p)$, whereas the corresponding ratios for profiles are $r' = rm(w)/N^{1/3}$ and $r'' = rm(s)/N^{2/3}$ (on the other hand, the areal and lineal fractions of small cells remain constant and equal to their volume fraction p). A simple calculation then gives

$$(5a) \quad \mathbf{E}v'^2 = \mathbf{E}V'^2 \frac{(pN^{-2/3}m(w)m(v'^2) + (1-p))[1 + p(N-1)]^{4/3}}{pN^{2/3}m(w) + (1-p)},$$

$$(5b) \quad \mathbf{E}v''^2 = \mathbf{E}V''^2 \frac{(pN^{-1/3}m(s)m(v''^2) - (1-p))[1 + p(N-1)]^{2/3}}{pN^{1/3}m(s) + (1-p)}.$$

The maximum values are again attained at $p \approx 0.5$ —Fig. 2. However, whereas CV v is nearly equal in both the BePG, BePS tessellations, other coefficients of variation have considerably higher values in BePS tessellations and the corresponding difference is greater at higher values of N ($\approx 35\%$ for CV v' and 27% for CV v'' at $N = 70$). The cause is the loss of inner cell profiles and the increase of outer cell and profile size with growing N in BePG tessellations (there is only ≈ 80 outer cells and ≈ 120 inner ones in a 3D fragmented cell at $N = 200$).

Summarizing, all important size characteristics of a tessellation generated by Bernoulli cluster fields with moderate cluster size can be approximately calculated from the characteristics of the tessellations generated by the corresponding Neyman-Scott cluster field ($p = 1$) and of PVT ($p = 0$). The input data are as follows: mean breadth $\mathbf{E}w$, surface area $\mathbf{E}s$ and three cell and profile second moments about the origin $\mathbf{E}v^2$, $\mathbf{E}v'^2$, $\mathbf{E}v''^2$ —see Tab. 1.

| N | BePG | | | | | BePS | | | | |
|-----|---------------|---------------|-----------------|------------------|-------------------|---------------|---------------|-----------------|------------------|-------------------|
| | $\mathbf{E}w$ | $\mathbf{E}s$ | $\mathbf{E}v^2$ | $\mathbf{E}v'^2$ | $\mathbf{E}v''^2$ | $\mathbf{E}w$ | $\mathbf{E}s$ | $\mathbf{E}v^2$ | $\mathbf{E}v'^2$ | $\mathbf{E}v''^2$ |
| 30 | 1.14 | 5.09 | 4.00 | 1.90 | 1.038 | 1.60 | 6.17 | 2.26 | 0.90 | 0.675 |
| 50 | 1.03 | 4.76 | 5.03 | 2.42 | 1.14 | 1.69 | 6.33 | 2.41 | 0.874 | 0.660 |
| 70 | 0.96 | 4.60 | 6.08 | 2.91 | 1.25 | 1.77 | 6.48 | 2.49 | 0.841 | 0.635 |
| 99 | 0.90 | 4.38 | 7.16 | 3.45 | 1.37 | 1.87 | 6.63 | 2.52 | 0.787 | 0.610 |
| 200 | 0.78 | 4.09 | 10.55 | 5.04 | 1.68 | 2.13 | 7.04 | 2.76 | 0.707 | 0.575 |
| PVT | 1.485 | 5.821 | 1.18 | 0.697 | 0.631 | — | — | — | — | — |

Table 1. Input data for calculating size characteristics of selected tessellations generated by Bernoulli cluster fields; $\delta = 0.05$.

3. RESULTS OF SIMULATIONS

The incremental method with the nearest neighbour algorithm [4] was used to construct the Voronoi tessellation associated with point fields of examined types. The tessellations generated by spherical cluster fields would not be normal because cells generated by points of the same cluster have a common vertex at their parent point. In order to avoid this, all daughter points were given small i.i.d. random shifts ξ ; their distribution was 3-variate centred normal with the variance $\sigma^2 I$, $\sigma = 0.0002\varrho_p$, hence 250 times smaller than the value of $\delta = 0.05$. This value ensured tolerable stability of the construction. The point field was generated within a unit cube and a great care was given to the suppression of edge effects which can seriously influence the numerical results, in particular in tessellations with great dispersion of cell sizes. After removing the cells affected by cube edges, usually about 10^3 cells per a realization remained for the statistical analysis. For tessellations generated by Neyman-Scott cluster fields (i.e. $p = 1$), the average number of realizations was about 10^3 , hence the values in Tab. 1 are based on average on 2×10^6 3D cells and on approximately the same number of the 2D and 1D profiles for each choice of N .

The construction of tessellations generated by Bernoulli cluster fields was more difficult due to considerably lowered stability, particularly in the case of BePS tessellations with high N . The numbers of examined cells and profiles were typically between 10^5 and 10^6 cells for BePG cluster fields and between 3×10^4 and 10^5 for BePS fields.

Simulated $\{\mathbf{E}w, \mathbf{E}s\}$ curves lie systematically within the loops calculated by the approximate numerical approach, however the deflection is small at $\delta = 0.05$. It does not exceed 10% even at $\delta = 0.5$, but the numerical model is completely wrong at $\delta = 2$ —Fig. 5.

Values of the coefficients of variation obtained by numerical approximation and by simulations are in a very good agreement in the case of CV v and the mutual

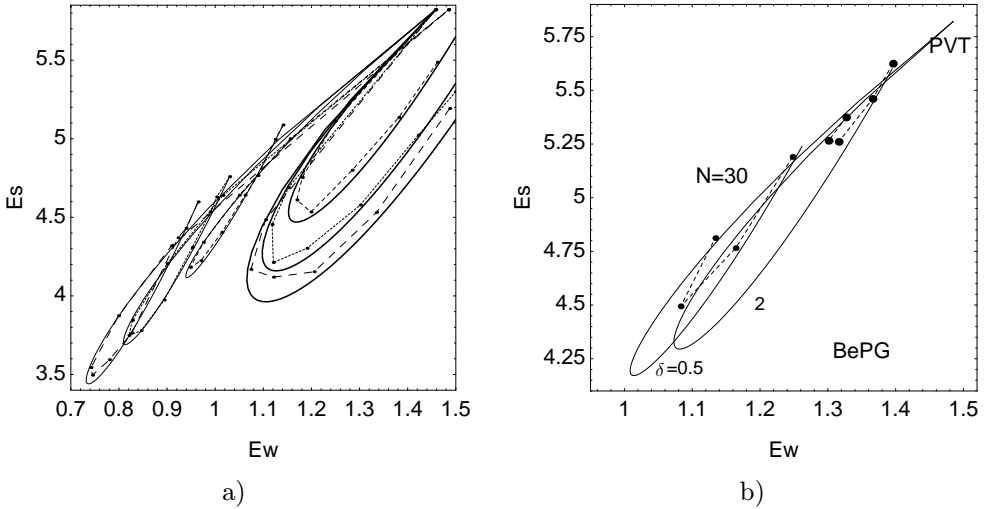


Figure 5. A comparison of calculated $\{Ew, Es\}$ values (full lines) with the results of computer simulations: a) $\delta = 0.05$; only the central part of Fig. 3 is shown, b) the partial and complete breakdown of the calculations by Eq. 3 at $\delta = 0.5, 2$.

differences, which are clearly systematic (see Fig. 2), are higher at higher values of p , where large cells and profiles are infrequent and, consequently, improperly sampled. In any case, the error is rather in the simulated values than in the calculation.

The proposed model considerably widens the spectrum of tessellations available up to now. The calculations of 3D grain size characteristics have been based nearly exclusively on monohedral and quasi-monohedral tessellations and on PVT (for review see [5]). The only exception was the Johnson-Mehl model [2] in a detailed study by Horálek [1]; the whole Johnson-Mehl model is described in the $w-s$ diagram by a curve starting at the PVT point, passing between the BePG and BePS loops and ending at $Ew \approx 0.9$, $Es \approx 3.9$ (with CV $v \rightarrow \infty$). In contrast to this, the present model is practically unlimited and fills an appreciable area in the $\{w, s\}$ plane. Also the coefficients of variation have only the lower bounds and no singularities except in the origin.

The relations of the present model to the estimation of the grain size as represented by various National Standards (see Vander Voort [14]) are discussed in [8], [10], [13], [15], its application to the simulation of intercrystalline crack growth is described in [9].

References

- [1] V. Horálek: ASTM grain size model and related random tessellation models. *Materials Characterization* 25 (1990), 263–284.
- [2] J. Møller: Random Johnson-Mehl tessellations. *Adv. in Appl. Probab.* 24 (1992), 814–844.
- [3] J. Møller: *Lectures on Random Voronoi Tessellations*. Lecture Notes in Statistics 87. Springer-Verlag, New York, 1994.
- [4] A. Okabe, B. Boots and K. Sugihara: *Spatial Tessellations*. J. Wiley & Sons, Chichester, 1992.
- [5] P. Ponižil, I. Saxl: Grain size estimation II: Other models, variances. In: STER-MAT'2000, Proceedings of the Sixth Int. Conf. "Stereology and Image Analysis in Materials Science" (L. Wojnar, K. Roźniatowski, eds.). Polish Society for Stereology, Cracow, 2000, pp. 379–384.
- [6] I. Saxl, P. Ponižil: 3D Voronoi tessellations of cluster fields. *Acta Stereol.* 17 (1998), 237–246.
- [7] I. Saxl, P. Ponižil: 3D Voronoi tessellations generated by Poisson and lattice of cluster fields. *Acta Stereol.* 17 (1998), 247–252.
- [8] I. Saxl, P. Ponižil: Random tessellations: Stochastic simulations and applications. Proceedings of the workshop "Programs and Algorithms of Numerical Mathematics", Libverda 2000. Mathematical Institute of the Academy of Sciences of the Czech Republic, Praha, 2000, pp. 150–161.
- [9] I. Saxl, K. Sülleiová and P. Ponižil: 3D simulations of intergranular fracture. In: Proceedings of the International Conference "Fractography 2000", Vysoké Tatry, 15–18. 10. 2000 (L. Parilák, ed.). Inst. Mat. Res., Slovak Acad. Sci., Košice, 2000, pp. 94–107.
- [10] I. Saxl, K. Sülleiová and P. Ponižil: Simulating grain size estimation. *Metallic Materials* 39 (2001), 396–409.
- [11] D. Stoyan, W. S. Kendall and J. Mecke: *Stochastic Geometry and its Applications*. J. Wiley & Sons, New York, 1995.
- [12] D. Stoyan, H. Stoyan: *Fractals, Random Shapes and Point Fields*. J. Wiley & Sons, Chichester, 1994.
- [13] A. Ševčík, K. Sülleiová, M. Besterci, I. Kohútek and I. Saxl: Grain size estimation in steels. *Metallic Materials* 40 (2002), in press.
- [14] G. F. Vander Voort: Grain size measurement. In: *Practical Applications of Quantitative Metallography*. ASTM STP 839, ASTM, Philadelphia, 1982, pp. 85–131.
- [15] O. Velgosová, I. Saxl and M. Besterci: Microstructural characteristics of dispersion strengthened Cu-based system. In: Proc. 3rd International Conference "Materials Structure & Micromechanics of Fracture" (P. Šandera, ed.). Vutim, Brno University of Technology, 2001, pp. 223–231, CD ROM.

Authors' addresses: I. Saxl, Mathematical Institute, Academy of Sciences of the Czech Republic, Žitná 25, CZ 115 67 Praha 1, Czech Republic, e-mail: saxl@math.cas.cz; P. Ponižil, Tomas Bata University in Zlín, Náměstí TGM 275, CZ 762 72 Zlín, Czech Republic, e-mail: ponizil@ft.utb.cz.